JVST A
Journal of Vacuum Science & Technology A

ARTICLE

pubs.aip.org/avs/jva

Structural, electronic, and thermodynamic properties of Li_3X (X = N, P, As) compounds for solid-state lithium-ion batteries

Cite as: J. Vac. Sci. Technol. A 43, 052801 (2025); doi: 10.1116/6.0004732
Submitted: 23 May 2025 · Accepted: 18 July 2025 ·
Published Online: 6 August 2025

A. Benamrani,[1] M. A. Ghebouli,[2,3] Faisal Katib Alanazi,[4] M. Fatmi,[2,a)] B. Ghebouli,[5] S. Alomairy,[6] and M. Çakmak[7,8]

AFFILIATIONS

[1]Laboratory of Materials Physics, Radiation and Nanostructure (LPMRN), University Mohamed El Bachir El Ibrahimi of Bordj Bou-rreridj, Bordj Bou-Arreridj 34000, Algeria
[2]Research Unit on Emerging Materials (RUEM), University Ferhat Abbas of Setif 1, Setif 19000, Algeria
[3]Department of Chemistry, Faculty of Sciences, University of M'sila University Pole, Road Bourdj Bou Arreiridj, M'sila 28000, Algeria
[4]Department of Physics, College of Sciences, Northern Border University Arar, Arar 73222, Saudi Arabia
[5]Laboratory for the Study of Surfaces and Interfaces of Solid Materials (LESIMS), University Ferhat Abbas of Setif 1, Setif 19000, Algeria
[6]Department of Physics, College of Science, Taif University, Taif 21944, Saudi Arabia
[7]7Department of Photonics, Faculty of Applied Sciences, Gazi University, Ankara, 06500, Turkey
[8]Photonics Application and Research Center, Gazi University, 06500 Ankara, Turkey

[a)]**Author to whom correspondence should be addressed:** fatmimessaoud@yahoo.fr

ABSTRACT

This study investigates the structural, electronic, mechanical, and thermodynamic properties of Li_3X compounds (where X represents nitrogen, phosphorus, and arsenic) using first-principles calculations based on density functional theory. Calculations were performed using the QUANTUM ESPRESSO package within the generalized gradient approximation framework with DFT-D3 dispersion correction to account for van der Waals interactions. Results show systematic trends in the hexagonal crystal structure, with lattice parameters increasing and bulk modulus values decreasing significantly from Li_3N to Li_3P to Li_3As. Elastic constant analysis reveals decreasing values across all constants, with C_{13} showing the most dramatic reduction, indicating reduced mechanical coupling between axes. The B/G ratios (1.51, 1.17, and 1.17 for Li_3N, Li_3P, and Li_3As, respectively) classify all three compounds as brittle materials according to Pugh's criterion. Electronic structure analysis demonstrates a transition from predominantly ionic bonding in Li_3N to more covalent character in Li_3P and Li_3As, manifested in decreasing bandgaps (1.1 eV to 0.7 eV to 0.65 eV) and increased orbital hybridization. Thermodynamic properties studied through the quasi-harmonic approximation show differences in vibrational energy, entropy (with Li_3As exhibiting the highest values), and isochoric heat capacity (approaching the Dulong–Petit limit at high temperatures). This study provides crucial insights into the relationship between atomic structure and physical properties of these compounds, thereby highlighting their potential in energy storage and thermoelectric applications.

I. INTRODUCTION

Lithium compounds are materials of profound importance in many contemporary technological applications, particularly in the fields of energy storage and conversion.[1,2] Lithium nitride (Li_3N) receives special attention due to its distinctive properties as a superionic conductor, making it a promising material for use in electrolytic solutions for lithium cells and as a hydrogen storage medium.[1] Li_3N features a layered structure with two plane types: Li_2N planes (containing lithium and nitrogen ions) and Li planes (containing only lithium ions). Studies reveal that lithium ions

move readily within Li_2N planes but have limited mobility in Li planes and along the *c* axis—a conductivity variation linked to the chemical bonding and electronic states of the moving ions.[3] Similar to Li_3N, lithium phosphide (Li_3P) has emerged as a promising lithium-ion conductor with applications in solid-state lithium batteries.[4] The electronic structure of Li_3P exhibits important similarities to Li_3N, with both materials demonstrating ionic character. A unique feature of Li_3P is that its constituent layers (Li_2P and Li monolayers) are metallic when separated, but undergo a metal–insulator transition when the interplane distance falls below 4.24 Å, with charge transfer from Li to P playing a crucial role in its stability and conductive properties.[5] Li_3N decomposes below 0.5 V, while Li_3P remains stable up to 2.2 V, making it more suitable for higher voltage applications.[6] These compounds are hard, brittle, and dark brown in color. They are sensitive to air and moisture. Fine powders of Li_3N and Li_3P can ignite in high humidity environments.[6] In contrast, Ni_3Al exhibits unique mechanical properties that make it attractive for structural applications, especially in high temperature and pressure applications such as diesel engine turbocharger rotors, high-temperature dies and molds, hydroturbines, and cutting tools.[7] The Li_3X family, where *X* represents group 15 elements (N, P, and As), forms an interesting subject in materials science due to their unique ionic and electronic conductivity properties. These compounds demonstrate the interesting transition from predominantly ionic to more metallic behavior as we move down group 15 from nitrogen to arsenic. The reactivity of these compounds with air and moisture presents significant challenges for their practical application but also reflects their interesting chemical properties. All three compounds require special handling techniques due to their high reactivity, necessitating storage, and manipulation under inert atmospheres to prevent rapid decomposition. Recent computational studies have focused on understanding the electronic structure of these materials at the atomic level, which has led to important insights regarding their conductivity mechanisms and potential for optimization through doping or partial substitution.[8] The anisotropic nature of the chemical bonds in Li_3X compounds is particularly noteworthy, as it creates unique pathways for ion transport that differ significantly between the in-plane and out-of-plane directions of the crystal structure.[9] Recent studies have demonstrated that nanostructured porous frameworks, particularly those based on graphene and silicene, play a pivotal role in enhancing the performance of lithium batteries by improving electrical conductivity, increasing surface area, and facilitating ion transport within the electrodes. A comprehensive review highlighted that porous graphene structures, such as aerogels and foams, significantly improve specific capacity and cycling stability due to their high conductivity and open architecture.[10] On the theoretical side, density functional theory (DFT) calculations have shown that porous silicene and silicon graphenylenelike surfaces possess promising electronic and mechanical properties suitable for energy storage applications, including their use as anode materials in lithium batteries.[11] Moreover, recent experimental work on laser-induced porous graphene revealed the formation of three-dimensional conductive frameworks with excellent electrochemical performance as lithium battery electrodes.[12] Additionally, other studies demonstrated that passivated porous graphene phases exhibit highly stable and tunable nanostructures, making them suitable for advanced applications requiring precise surface control, with potential implications for electrochemical systems.[13] A recent first-principles study further indicated that nanoporous graphene exhibits strong lithium adsorption capabilities due to its open structure and high surface reactivity, positioning it as a promising material for future energy storage systems.[14] Based on these findings, integrating Li_3X (X = N, P, As) compounds with such porous frameworks could provide a promising pathway toward the development of high-performance solid-state lithium batteries. Therefore, in this work, we systematically investigate the structural, electronic, and ionic transport properties of Li_3X (X = N, P, As) compounds using first-principles calculations. Our aim is to evaluate their potential as solid-state electrolytes for lithium batteries by analyzing their thermodynamic stability, electronic bandgaps, and lithium-ion mobility. This study provides a comparative insight into the impact of anion substitution on the performance of Li_3X compounds, highlighting their suitability for next-generation all-solid-state lithium battery applications.

II. COMPUTATIONAL METHOD

First-principles calculations based on density functional theory (DFT) were performed using the QUANTUM ESPRESSO package,[15] which is an integrated suite of open-source computer codes for electronic-structure calculations and materials modeling. The calculations were carried out within the framework of the generalized gradient approximation (GGA) using the Perdew–Burke–Ernzerhof (PBE) exchange-correlation functional.[16] To account for van der Waals interactions, which are particularly important in layered structures, Grimme's DFT-D3 dispersion correction was applied.[17] The electron–ion interactions were described using ultrasoft pseudopotentials from the Standard Solid-State Pseudopotentials (SSSP) library.[18] The wavefunctions were expanded in plane waves with a kinetic energy cut-off of 80 Ry for the wavefunctions and 800 Ry for the charge density. For the Brillouin zone integration, a Monkhorst–Pack *k*-point mesh[19] of $12 \times 12 \times 12$ was used for the bulk calculations. The electronic configurations of the atoms involved in the Li_3X compounds can be represented in terms of noble gas notation as follows: lithium (Li): [He] $2s^1$, nitrogen (N): [He] $2s^2$ $2p^3$, phosphorus (P): [Ne] $3s^2$ $3p^3$, and arsenic (As): [Ar] $3d^{10}$ $4s^2$ $4p^3$. For Li_3N, Li_3P, and Li_3As, the convergence criteria for self-consistent field calculations were set to 10^{-6} Ry for the total energy and 10^{-5} Ry/Bohr for the forces on atoms during structural optimization.[20] The elastic properties were determined using the stress–strain. This approach involves applying small deformations to the equilibrium crystal structure and calculating the resulting stress tensors.[21] The relationship between stress (σ) and strain (ε) provides the elastic constants through Hooke's law $\sigma_{ij} = C_{ijkl} \times \varepsilon$, where C_{ijkl} represents the elastic constant tensor. The thermodynamic properties were calculated using the quasi-harmonic approximation approach, which extends beyond the harmonic approximation by including volume-dependent phonon frequencies. This approach is essential for describing volume-dependent thermal effects such as thermal expansion.[22]

III. RESULTS AND DISCUSSION

A. Structural properties

Figure 1 depicts the hexagonal crystal structure of Li_3X compounds (space group P6/mmm), where X represents group 15 elements (N, P, or As). These structures feature alternating Li_2X and pure Li layers perpendicular to the c axis. X atoms occupy the Wyckoff position 1a (0,0,0), while lithium atoms occupy two distinct sites: Li(1) at position 1b (0,0,1/2) aligned along the c axis and Li(2) at position 2c (1/3,2/3,0) arranged trigonally in the X-plane. Each X atom is coordinated by eight Li atoms—six Li(2) atoms forming a trigonal prism in-plane (shown as orange triangular faces) and two Li(1) atoms positioned axially. When nitrogen is systematically substituted by phosphorus or arsenic, the lattice parameters expand anisotropically and bond character evolves from predominantly ionic to more covalent, affecting electronic, mechanical, and thermal properties while maintaining the same structural framework.

Figure 2 presents the total energy variation as a function of volume for Li_3X (X = N, P, As) compounds in the α-hexagonal phase, providing crucial insights into their structural stability and mechanical properties. The energy–volume curves exhibit parabolic shapes near their minima with distinctive asymmetry (steeper slopes at smaller volumes), demonstrating the characteristic anharmonic behavior during compression versus expansion. The equilibrium volumes increase progressively from Li_3N [see Fig. 2(c)] to Li_3P [see Fig. 2(b)] to Li_3As [see Fig. 2(a)], corresponding to the increasing atomic radii down group 15. The Birch–Murnaghan equation of state effectively captures these relationships, allowing precise determination of equilibrium parameters that reveal how these materials' resistance to compression. The Birch–Murnaghan equation of state represents one of the most important theoretical frameworks for describing the relationship between pressure and volume in crystalline solids.[23] The equation is grounded in fundamental principles of continuum mechanics and finite elastic strain theory, making it particularly suitable for describing materials under compression.

The third-order Birch–Murnaghan equation of state for energy as a function of volume can be written as follows:

$$E(V) = E_0 + \frac{9V_0B_0}{16}\left\{\left[\left(\frac{V_0}{V}\right)^{2/3} - 1\right]^3 B'_0 + \left[\left(\frac{V_0}{V}\right)^{2/3} - 1\right]^2 \times \left[6 - 4\left(\frac{V_0}{V}\right)^{2/3}\right]\right\}. \quad (1)$$

Here, $E(V)$ is the total energy of the system at volume V, E_0 the total energy of the system at the equilibrium volume, V the current volume of the crystal cell, V_0 the equilibrium (reference) volume of the crystal cell at zero pressure, B_0 the bulk modulus at the equilibrium volume, typically measured in GPa and B_0' the first pressure derivative of the bulk modulus at the equilibrium volume (dimensionless).The structural and mechanical properties of Li_3X (X = N, P, As) compounds reveal systematic trends as we move down group 15 of the periodic table. As shown in Table I, our calculated lattice parameters demonstrate progressive expansion of the hexagonal unit cell as the atomic radius increases from nitrogen to arsenic.

Our calculated values for Li_3N closely match those reported by Hossain *et al.*,[24] confirming the reliability of our computational approach. The c/a ratios (1.769–1.795) increase slightly across the series, indicating growing structural anisotropy. Most notably, the bulk modulus decreases substantially from Li_3N (66.6 GPa) to Li_3P (41.2 GPa) to Li_3As (36.3 GPa), while B_0' values increase modestly (4.14–4.43).Compared to similar nitrides like Mg_3N_2 (B_0 = 114 GPa)[25] and Ca_3N_2 (B_0 = 81 GPa),[26] Li_3N exhibits lower incompressibility due to lithium's smaller ionic radius and weaker

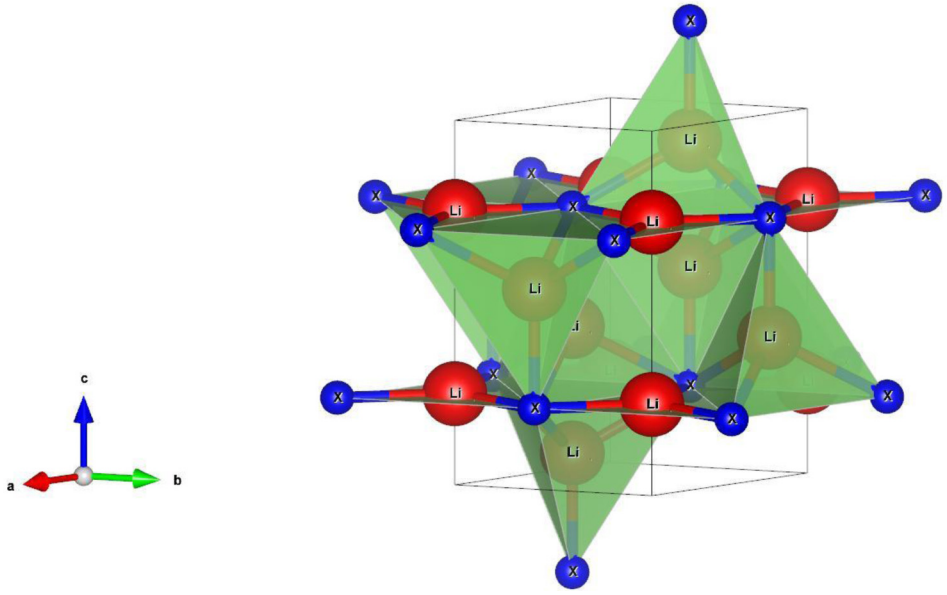

FIG. 1. Hexagonal structure of Li_3X (X = As, P, and N), Lithium atoms are represented by lighter-shaded balls, while X atoms (X = As, P, and N) are represented by darker-shaded balls.

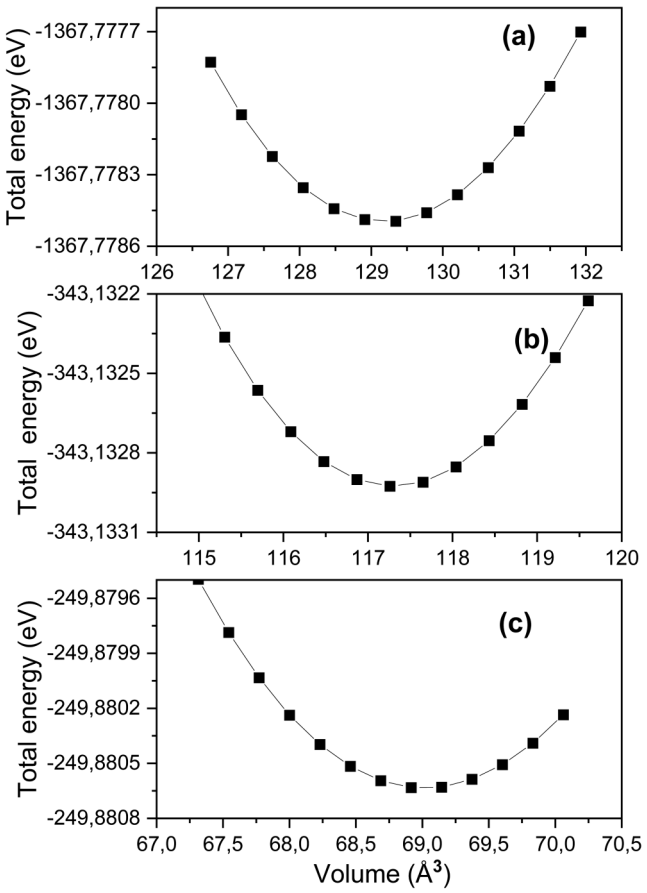

FIG. 2. Energy variation vs volume of Li_3X (X = N, P, As) compounds' atα-hexagonal phase. (a), (b), and (c) correspond to Li_3As, Li_3P, and Li_3N, respectively.

bonding. These compounds follow similar trends to other group I–V materials like Na_3Sb (B_0 = 34 GPa)[27] and K_3Bi (B_0 = 25 GPa),[28] where increasing atomic size of both cation and anion further reduces the bulk modulus. When fitted to the Birch–Murnaghan equation of state, our energy–volume data provide reliable mechanical parameters that correlate with the bonding character evolution from more ionic in Li_3N to increasingly covalent in Li_3P and Li_3As,[29] consistent with other theoretical studies of crystal structure mechanics under compression.[30] The decreasing bulk modulus trend across the series indicates that these materials become progressively more compressible as the group 15 element becomes heavier, which has important implications for their potential applications in energy storage and other technologies.

B. Elastic constants

Six different strain patterns were applied to the optimized structure to capture all independent elastic constants.[31] For each pattern, multiple strain magnitudes (typically ranging from −2% to +2% in steps of 0.5%) were used to ensure linearity in the stress–strain relationship.[32] For each strained configuration, a single-point calculation was performed to determine the stress tensor. The stress was calculated using the stress theorem implemented in QUANTUM ESPRESSO, which provides the stress components directly from the electronic structure.[33] The linear stress contribution was obtained by fitting the stress–strain curves for each component, and the independent elastic constants were calculated as the least-squares solution to a linear system of equations,[34] considering the crystal symmetry of the Li_3X compounds. For hexagonal structures like Li_3N, there are five independent elastic constants (C_{11}, C_{12}, C_{13}, C_{33}, and C_{44}). The elastic properties of Li_3X (X = N, P, As) compounds reveal significant trends and correlations as we move down group 15 of the periodic table. All elastic constants (C_{11}, C_{12}, C_{13}, C_{33}, C_{44}, C_{66}) systematically decrease from Li_3N to Li_3P to Li_3As, reflecting the weakening of interatomic bonding as the atomic radius and mass increase.[35] The most dramatic reduction is observed in C_{13}, which drops from 16.08 GPa in Li_3N to merely 2.60 GPa in Li_3As, indicating substantially reduced mechanical coupling between the a axis and c axis deformations.[36] The pronounced difference between C_{33} and C_{11} values, particularly in Li_3N (180.7 versus 123.6 GPa), confirms the strong anisotropic nature of these hexagonal compounds, with greater stiffness along the c axis compared to the a axis.[37] This anisotropy diminishes considerably in Li_3P and Li_3As, where the C_{33}/C_{11} ratio decreases from 1.46 in Li_3N to 1.04 in Li_3P and 1.02 in Li_3As, suggesting more uniform bonding in the heavier compounds.[38] The bulk modulus values of 66.52, 39.73, and 34.41 GPa for Li_3N, Li_3P, and Li_3As, respectively, exhibit a steep decline across the series, with Li_3N's value matching closely with the 67 GPa reported by Hossain *et al.*[24] This pronounced decrease (approximately 40% reduction from Li_3N to Li_3P and a further 13% from Li_3P to Li_3As) confirms the substantial decrease in resistance to volume change as nitrogen

TABLE I. Calculated equilibrium lattice constants a_0, c_0 in (Å), c_0/a_0 ratio, bulk modulus B_0 in (GPa), pressure derivative of bulk modulus B' of Li_3N, Li_3P, and Li_3As at the hexagonal β phase. Lattice parameters a_0 and c_0 are calculated using geometry optimization, while B_0 and B' are calculated by fitting of energy–volume curves to the third-order Birch–Murnaghan equation of state.

Compound		a_0 (Å)	c_0 (Å)	c_0/a_0	B_0 (GPa)	B'	Reference
Li_3N	Present work	3.552	6.285	1.769	66.6	4.14	
	Others	3.579	6.360	1.777			24
Li_3P	Present work	4.228	7.572	1.791	41.2	4.28	
Li_3As	Present work	4.365	7.836	1.795	36.3	4.43	

is substituted with larger phosphorus and arsenic atoms.[39] When compared to similar materials, Li_3N shows significantly lower elastic constants than binary nitrides like AlN (C_{11} = 304 GPa) and GaN (C_{11} = 293 GPa),[40] but higher than alkali metal pnictides such as Na_3Sb ($B \approx 32$ GPa). The trend observed in Li_3X compounds is consistent with other lithium-based materials; for instance, lithium silicides ($Li_{22}Si_5$) exhibit bulk moduli in the range of 35–40 GPa.[41] The calculated bulk-to-shear modulus ratios (B/G) are 1.51, 1.17, and 1.17 for Li_3N, Li_3P, and Li_3As, respectively. According to Pugh's criterion, materials with $B/G < 1.75$ are predicted to be brittle,[42] indicating that all three compounds are brittle materials, with Li_3P and Li_3As being more brittle than Li_3N, consistent with experimental observations.[43] The Poisson's ratio (ν) decreases significantly from Li_3N (0.227) to Li_3P (0.167) and remains nearly constant for Li_3As (0.166). This decline suggests a transition in bonding character, with Li_3N showing more metalliclike bonding while Li_3P and Li_3As demonstrate more covalentlike bonding.[44] The Debye temperature (θD) and sound velocity (vm) both decrease substantially across the series, with θD dropping from 5599.40 K to 3773.88 K and vm declining from 814.11 to 444.36 m/s. These reductions correlate with increasing atomic mass and decreasing bond strength, directly affecting phonon propagation and thermal properties.[45] The exceptionally low sound velocity in Li_3As makes it particularly promising for thermoelectric applications due to potentially low lattice thermal conductivity.[46]

C. Electronic characterization

Figure 3(a) shows the band structure and PDOS of Li_3N. A direct bandgap of approximately 1.1 eV is observed, with relatively flat valence bands indicating localized nitrogen states and limited hole mobility. The PDOS displays distinct separation between Li and As orbitals, confirming the predominantly ionic bonding character in this compound. Figure 3(b) presents the case of Li_3P, which features a narrower indirect bandgap of about 0.7 eV between the Γ and K points. The increased band dispersion suggests better carrier mobility, and the PDOS reveals significant hybridization between P and Li states, particularly in the energy range from −2 to −5 eV. This indicates a shift toward a more covalent bonding nature compared to Li_3N. Figure 3(c) corresponds to Li_3As, showing the smallest bandgap of approximately 0.65 eV. It exhibits the most dispersed band structure, along with enhanced hybridization near the Fermi level. The PDOS reflects a pronounced overlap of Li and N states, suggesting a predominantly covalent–metallic bonding character. This electronic configuration is favorable for thermoelectric performance due to high Seebeck coefficients and low lattice thermal conductivity.

The evolution of these electronic properties correlates directly with the structural and mechanical characteristics: the decreasing bandgap parallels the reduction in bulk modulus (66.52, 39.73, and 34.41 GPa) and increasing thermoelectric performance (with ZT values reaching 1.13 for p-type doped Li_3As).[47] Crystallographically, the space group evolution from P6/mmm for Li_3N to P63/mmc for Li_3P and Li_3As affects the electronic structure through altered atomic arrangements. The DOS analysis in Fig. 3 clearly demonstrates the bonding transition from predominantly ionic in Li_3N (with distinct separation between N and Li states) to increasingly covalent-metallic

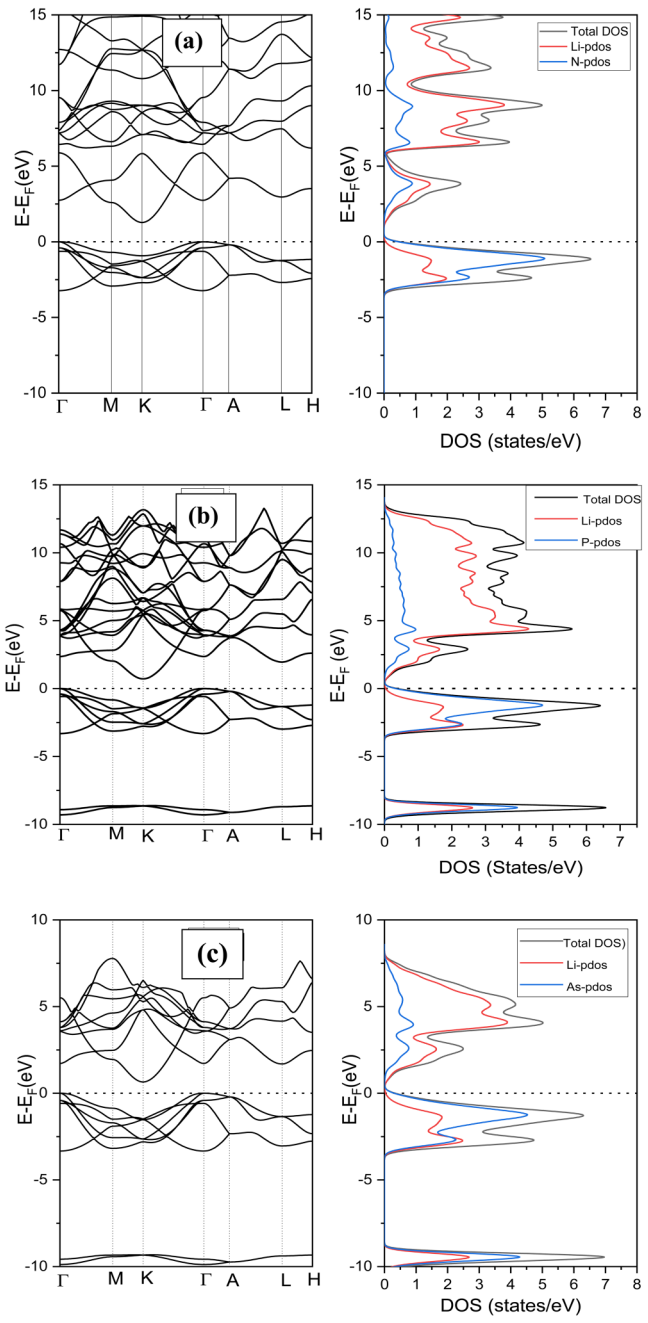

FIG. 3. Electronic band structure (left) and projected density of states (PDOS) (right) of Li_3X compounds: (a) Li_3N, (b) Li_3P, and (c) Li_3As.

character in Li_3P and Li_3As (with enhanced orbital hybridization).[48] These electronic structure differences explain why Li_3N exhibits superior ionic conductivity ideal for battery applications, while Li_3P and especially Li_3As show more promise for thermoelectric applications due to their advantageous band structures and extremely low

thermal conductivities. The systematic changes in electronic properties across this series provide valuable guidance for tailoring these materials for specific technological applications through compositional engineering and defect management.

D. Thermodynamic properties

1. Vibrational energy and vibrational free energy

Figure 4 illustrates the critical relationship between temperature and two fundamental thermodynamic parameters: vibrational energy and vibrational free energy for the Li_3X compound family, providing profound insights into their thermal behavior and stability. At the microscopic level, atoms in these crystalline solids vibrate around their equilibrium positions, with these vibrations quantized as phonons quantum mechanical entities representing collective atomic oscillations. The vibrational energy curves show steadily increasing values with rising temperature, reflecting the growing thermal excitation of phonon modes as more energy becomes available to populate higher energy vibrational states, with the rate of increase being steepest at low temperatures and becoming more linear at higher temperatures. Conversely, the vibrational free energy ($F_{vib} = E_{vib} - TS_{vib}$) curves demonstrate a decreasing trend with increasing temperature because the entropic term ($-TS_{vib}$) becomes increasingly negative at higher temperatures, outweighing the increase in vibrational energy and representing the system's increasing disorder. The subtle but important differences between the curves for Li_3N, Li_3P, and Li_3As reflect their distinct bonding characteristics and atomic masses, with Li_3N's lighter nitrogen atoms and stronger ionic bonds typically exhibiting higher vibrational frequencies than its heavier analogs. These vibrational properties directly influence phase stability, thermal expansion, heat capacity and phonon transport (particularly relevant for Li_3P and Li_3As, which have promising thermoelectric properties due to their low lattice thermal conductivity values of approximately 2.83 and 2.80 W/m K at 300 K).[44]

2. Entropy

Figure 5 illustrates the crucial relationship between entropy (S) and temperature in the Li_3X (X = N, P, As) compound family, revealing fundamental thermodynamic behavior that governs these materials' stability and phase transformations. Entropy, a measure of the system's microscopic disorder, displays a characteristic monotonic increase with temperature across all three compounds, following the principles of the third law of thermodynamics. The entropy curves begin near zero at very low temperatures and rise progressively, with the most rapid increase occurring at lower temperature ranges (below 300 K) before the rate of increase gradually diminishes at higher temperatures, approaching a more linear behavior. The entropy values for the three compounds show a systematic trend, with Li_3As typically exhibiting the highest entropy at any given temperature, followed by Li_3P and then Li_3N with the lowest entropy. This ordering directly correlates with the atomic masses of the constituent elements, where heavier atoms generally lead to lower-frequency vibrational modes that contribute more significantly to entropy at a given temperature. Li_3N lower entropy reflects its stronger, more rigid ionic bonding and lighter nitrogen atoms, resulting in higher-frequency phonon modes that require more thermal energy to excite. The shape of these entropy curves provides valuable information about phase stability and transformations, as any change in slope or discontinuity would indicate a phase transition.[49]

3. Isochoric heat capacity C_V

Figure 6 illustrates the temperature dependence of isochoric heat capacity (C_V) for Li_3X (X = N, P, As) compounds, revealing crucial insights into their thermal and phonon behavior. The

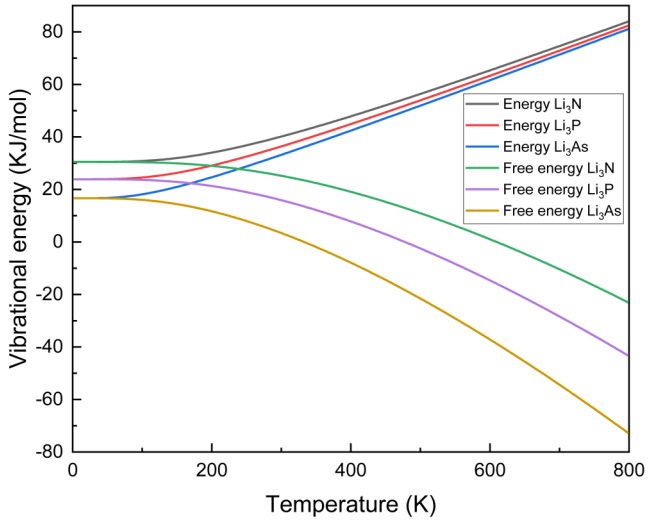

FIG. 4. Dependence with temperature of the vibrational energy and vibrational free energy in Li_3X (X = N, P, and As) materials.

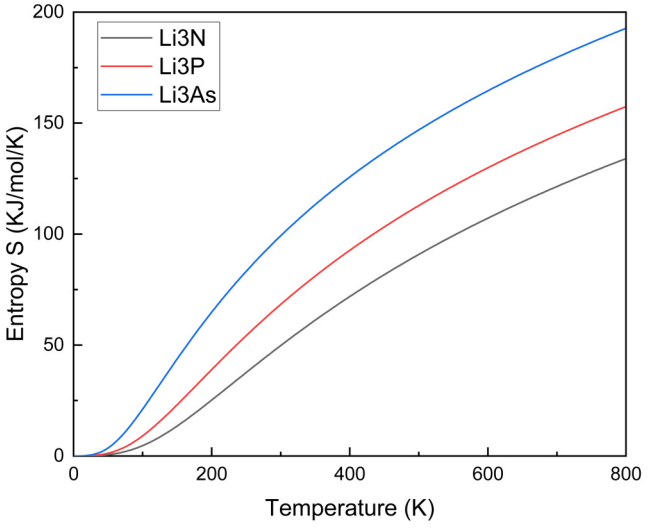

FIG. 5. Entropy S vs temperature in Li_3X (X = N, P, and As) materials.

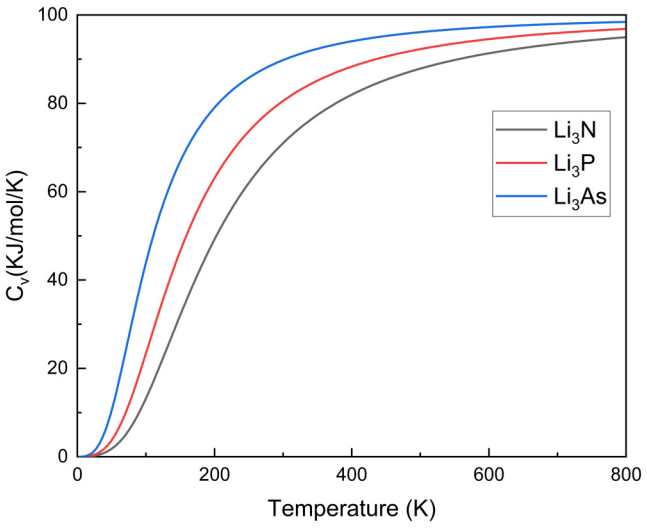

FIG. 6. Isochoric heat capacity C_V vs temperature in Li_3X (X = N, P, and As) materials.

isochoric heat capacity, which measures the amount of heat required to raise the temperature of a system at constant volume, is one of the most fundamental thermodynamic properties as it directly reflects the quantized energy states available to the system. The characteristic temperature evolution of heat capacity for crystalline solids, following quantum mechanical principles. At very low temperatures (approaching 0 K), the heat capacity approaches zero for all three compounds, consistent with the third law of thermodynamics. This occurs because at extremely low temperatures, thermal energy is insufficient to excite higher vibrational energy states, leaving only the lowest quantum states occupied. As temperature increases, the heat capacity rises rapidly in what is known as the quantum regime, where the temperature dependence approximately follows Debye's T^3 law. This cubic temperature dependence at low temperatures is a direct consequence of the quantum mechanical nature of phonons, the quantized lattice vibrations that dominate thermal properties in solids. The data show that Li_3As exhibits the highest heat capacity at low temperatures among the three compounds, followed by Li_3P and then Li_3N with the lowest values. This ordering correlates with the compounds' phonon density of states at low frequencies, which is influenced by the atomic masses and bond strengths. Heavier atoms (As > P > N) tend to vibrate at lower frequencies, resulting in more accessible vibrational states at a given low temperature and thus higher heat capacity. At intermediate temperatures, the curves show a transition region where the T^3 dependence gradually gives way to a more linear behavior. At high temperatures, all three compounds approach a limiting value known as the Dulong Petit limit,[50] where C_V tends toward $3R$ per mole of atoms (R is the gas constant).

IV. CONCLUSION

In this study, we conducted a comprehensive analysis of the structural, electronic, mechanical, and thermodynamic properties of Li_3X (X = N, P, As) compounds using first-principles calculations. The results reveal clear systematic trends across the series as we move from nitrogen to phosphorus to arsenic in group 15 of the periodic table. The structural properties show a progressive increase in lattice parameters from Li_3N to Li_3P to Li_3As, reflecting the increasing atomic radii and changes in bonding nature. In parallel, a significant decrease in bulk modulus from 66.6 GPa in Li_3N to 41.2 GPa in Li_3P to 36.3 GPa in Li_3As was observed, indicating that these materials become more compressible as the element size increases. The mechanical properties exhibit a systematic decrease in elastic constants across the series, with a notable reduction in the disparity between C_{33} and C_{11}, suggesting a decrease in structural anisotropy. The calculated B/G ratios indicate that all three compounds are brittle materials, with Li_3P and Li_3As being more brittle than Li_3N. Electronic structure analysis reveals a gradual transition from predominantly ionic bonding in Li_3N to more covalent character in Li_3P and Li_3As, with a decrease in bandgap from 1.1 eV in Li_3N to 0.7 eV in Li_3P and 0.65 eV in Li_3As. This trend correlates directly with differences in mechanical and thermal properties. The study of thermodynamic properties provides insight into the behavior of these compounds at different temperatures, showing expected trends in vibrational energy, free energy, entropy, and heat capacity. Li_3As exhibits the highest entropy and heat capacity values at low temperatures, followed by Li_3P and then Li_3N, a sequence that correlates with atomic masses and bond strengths.These findings provide valuable guidance for tailoring these materials for specific technological applications. The superionic conduction of Li_3N makes it suitable for battery applications, while Li_3P and especially Li_3As show promise for thermoelectric applications due to favorable band structures and extremely low thermal conductivities. Judicious modification of composition, such as partial substitution of nitrogen with phosphorus or arsenic in Li_3N, could lead to materials with optimized combinations of ionic and electronic conductivity, overcoming limitations of the pure compounds.

ACKNOWLEDGMENTS

The authors extend their appreciation to Taif University, Saudi Arabia, for supporting this work through Project No. TU-DSPP-2024-63.

AUTHOR DECLARATIONS

Conflict of Interest

The authors have no conflicts to disclose.

Author Contributions

A. Benamrani: Investigation (equal). **M. A. Ghebouli:** Software (equal). **Faisal Katib Alanazi:** Conceptualization (equal); Validation (equal). **M. Fatmi:** Validation (equal). **B. Ghebouli:** Formal analysis (equal). **S. Alomairy:** Formal analysis (equal). **M. Çakmak:** Data curation (equal).

DATA AVAILABILITY

Data underlying the results presented in this paper are not publicly available at this time but may be obtained from the corresponding author upon reasonable request.

REFERENCES

[1]A. Rabenau, Solid State Ionics **6**, 277 (1982).
[2]M. Fatmi, M. A. Ghebouli, B. Ghebouli, T. Chihi, S. Boucetta, and Z. K. Heiba, Rom. J. Phys. **56**, 935 (2011).
[3]B. A. Boukamp and R. A. Huggins, Phys. Lett. A **58**, 231 (1976).
[4]P. Giannozzi *et al.*, J. Chem. Phys. **152**, 154105 (2020).
[5]M. Seel and R. Pandey, MRS Proc. **210**, 155 (1990).
[6]G. Nazri and R. H. Muller, J. Electrochem. Soc. **132**, 2050 (1985).
[7]J. H. Westbrook and R. L. Fleischer, *Intermetallic Compounds: Principles and Practice*, 3rd ed. (Wiley, Chichester, UK, 2002), pp. 213–227.
[8]B. Ghebouli, M. A. Ghebouli, and M. Fatmi, Eur. Phys. J. Appl. Phys. **53**, 30101 (2011).
[9]T. Chihi, M. Fatmi, B. Ghebouli, and M. Guemmaz, Solid State Sci. **13**, 1414 (2011).
[10]O. Okhay and A. Tkach, J. Energy Storage **80**, 110336 (2024).
[11]G. S. L. Fabris, N. L. Marana, E. Longo, and J. R. Sambrano, Theor. Chem. Acc. **137**, 13 (2018).
[12]X. Ma, S. Wang, Z. Fu, H. Gao, Y. Shao, X. Li, and X. Yan, ACS Omega **10**, 11241 (2025).
[13]M. N. Sadeghi, P. Yazdanfar, and B. Rashidian, Opt. Mater. Express **11**, 2839 (2021).
[14]L. Barabanova and A. Buldum, Nanomaterials **14**, 1528 (2024).
[15]M. A. Ghebouli, K. Bouferrache, B. Ghebouli, M. Fatmi, Faisal K. Alanazi, and Talal M. Althagafi, RSC Adv. **15**, 26338 (2025).
[16]J. P. Perdew, K. Burke, and M. Ernzerhof, Phys. Rev. Lett. **77**, 3865 (1996).
[17]S. Grimme, J. Antony, S. Ehrlich, and H. Krieg, J. Chem. Phys. **132**, 154104 (2010).
[18]G. Prandini, A. Marrazzo, I. E. Castelli, N. Mounet, and N. Marzari, npj Comput. Mater. **4**, 72 (2018).
[19]L. Krache, M. A. Ghebouli, B. Ghebouli, M. Fatmi, T. Chihi, and S. I. Ahmed, Acta Phys. Pol. A **143**, 3 (2023).
[20]R. Boudissa *et al.*, Biochem. Biophys. Rep. **37**, 101601 (2024).
[21]B. Ghebouli, M. A. Ghebouli, M. Fatmi, N. Bouarissa, M. Benkerri, and I. A. Ibrahim, Acta Metall. Sin. **24**, 255 (2011).
[22]J. P. Perdew and A. Ruzsinszky, Rev. Mineral. Geochem. **71**, 1 (2010).
[23]F. Birch, Phys. Rev. **71**, 809 (1947).
[24]M. A. Hossain, A. K. M. A. Islam, and F. N. Islam, J. Sci. Res. **1**, 182 (2009).
[25]P. Rodriguez-Hernandez and A. Munoz, Semicond. Sci. Technol. **7**, 1437 (1992).
[26]G. Vaitheeswaran, V. Kanchana, and M. Rajagopalan, J. Alloys Compd. **336**, 46 (2002).
[27]V. Kanchana, G. Vaitheeswaran, and M. Rajagopalan, J. Alloys Compd. **359**, 66 (2003).
[28]A. Srivastava, M. Chauhan, and R. K. Singh, Phase Transit. **84**, 58 (2011).
[29]M. A. Ghebouli, T. Chihi, B. Ghebouli, and M. Fatmi, Chin. J. Phys. **56**, 323 (2018).
[30]F. Birch, J. Geophys. Res. **83**, 1257, https://doi.org/10.1029/JB083iB03p01257 (1978).
[31]L. Fast, J. M. Wills, B. Johansson, and O. Eriksson, Phys. Rev. B **51**, 17431 (1995).
[32]J. Zhao, J. M. Winey, and Y. M. Gupta, Phys. Rev. B **75**, 094105 (2007).
[33]O. H. Nielsen and R. M. Martin, Phys. Rev. Lett. **50**, 697 (1983).
[34]Y. Le Page and P. Saxe, Phys. Rev. B **65**, 104104 (2002).
[35]R. W. Hertzberg, R. P. Vinci, and J. L. Hertzberg, *Deformation and Fracture Mechanics of Engineering Materials* (Wiley, New York, 1996).
[36]M. Born and K. Huang, *Dynamical Theory of Crystal Lattices* (Oxford University, Oxford, UK, 1996).
[37]A. G. Every, *Second and Higher Order Elastic Constants* (Springer, Berlin, 1992).
[38]V. Wang, N. Xu, J. C. Liu, G. Tang, and W. T. Geng, Comput. Phys. Commun. **267**, 108033 (2021).
[39]G. Simmons and H. Wang, *Single Crystal Elastic Constants and Calculated Aggregate Properties: A Handbook*, 2nd ed. (MIT Press, Cambridge, MA, 1971).
[40]H. Schulz and K. H. Thiemann, Solid State Commun. **23**, 815 (1977).
[41]M. Amine Ghebouli, B. Ghebouli, T. Chihi, M. Fatmi, and A. Sameh Ibrahim, Mater. Sci. Semicond. Process. **135**, 106033 (2021).
[42]S. F. Pugh, London, Edinburgh, Dublin Philos. Mag. J. Sci. **45**, 823 (1954).
[43]G. Nazri, MRS Proc. **135**, 117 (1988).
[44]G. N. Greaves, A. L. Greer, R. S. Lakes, and T. Rouxel, Nat. Mater. **10**, 823 (2011).
[45]O. L. Anderson, J. Phys. Chem. Solids **24**, 909 (1963).
[46]Z. Zeng, C. Zhang, H. Yu, W. Li, Y. Pei, and Y. Chen, Mater. Today Phys. **21**, 100487 (2021).
[47]F. Wegner, F. Kamm, F. Pielnhofer, and A. Pfitzner, Z. Anorg. Allg. Chem. **649**, e202200330 (2022).
[48]A. Togo and I. Tanaka, Scr. Mater. **108**, 1 (2015).
[49]D. Bolmatov, V. V. Brazhkin, and K. Trachenko, Sci. Rep. **2**, 421 (2012).
[50]A. T. Petit and P. L. Dulong, Ann. Chim. Phys. **10**, 395 (1819), https://www.scirp.org/reference/referencespapers?referenceid=824448.